INFERRING SURFACE ROUGHNESS AND BREAKING WAVE PROPERTIES FROM POLARIMETRIC RADAR BACKSCATTERING

Paul A. Hwang[1] and Franco Fois[2]
[1]Remote Sensing Division, Naval Research Laboratory, Washington DC, USA
[2] Department of Geoscience and Remote Sensing, Delft University of Technology, the Netherlands

1. INTRODUCTION

Ocean surface roughness and surface wave breaking are two common parameters important to the studies of microwave ocean remote sensing and air-sea interactions. For example, remote sensing of ocean surface vector winds by radars and radiometers makes implicit use of the property that the normalized radar cross section (NRCS) and the sea surface brightness temperature are modified by the surface roughness and wave breaking; and both oceanographic properties are closely influenced by the wind. For air-sea interaction processes such as gas transfer or sea spray aerosol generation, the boundary layer turbulence properties are closely associated with the surface roughness, and wave breaking represents a dominate process of turbulence generation and air entrainment in the upper ocean layer.

It is difficult to obtain quantitative measurements of surface roughness and wave breaking using conventional oceanographic instruments, especially in high winds and inclement sea state conditions. Over the years, airborne and spaceborne scatterometers and polarimetric synthetic aperture radars (SARs) have produced a large amount of data for the construction of copolarized (*VV* and *HH*) and cross-polarized (*VH*) geophysical model functions (GMFs) with wind speed coverage ranging from mild to hurricane conditions. Because the response of microwave returns varies with the polarization, here we explore an empirical approach to derive the surface roughness and wave breaking information using the polarimetric differences of radar sea returns. The approach is described in Sec. 2, results and discussions are presented in Sec. 3, and a summary is given in Sec. 4.

2. APPROACH

The GMFs are treated as proxies of global ocean data of surface roughness and wave breaking reflected on the radar backscattering. The NRCS can be considered as made up of three broad components: (i) scattering from the tilted surface roughness component in Bragg resonance with the radar waves; (ii) the non-Bragg scattering from bubble plume features and discrete steep waveforms associated with wave breaking occurrences; and (iii) the modification of the relative permittivity from breaking-entrained air. The breaking causes three main changes: relative permittivity, surface roughness in the Bragg resonance portion, and non-Bragg scattering from bubble feature and surface geometry.

Extensive studies have established that the VV is dominated by Bragg scattering, which provides the information of sea surface roughness. The surface roughness reflected in the VV Bragg resonance consideration includes both components of direct wind generation and breaking disturbances. For practical purposes, they are classified as surface roughness without distinction of the generation sources. HH and VH have higher degrees of breaking contributions from non-Bragg scattering mechanisms that are incidence angle and wind speed dependent.

We propose to use the second order small slope approximation (SSA2) solution (Voronovich, 1994) to compute the roughness Bragg contributions of VV, HH and VH. The difference between GMFs and SSA2 solutions can then be used to construct an empirical model of breaking wave contribution to the radar backscattering. The version of the SSA2 solution described in Fois et al. (2014) is used in this work.

For the relative permittivity modification, an equivalent medium approach using the mixed rule as described in Hwang (2012) is adapted. Basically, the relative permittivity differs significantly in air and in water for microwave frequencies; therefore even a small amount of air can produce a large change in the relative permittivity of the resulting mixture. To account for the effect of entrained air, ideally we need to know the fraction of air in water (void fraction) and the vertical distribution of the bubble clouds carrying the air into water.

Considering the lack of such detail information of the bubble cloud distribution in the ocean and the small penetration depth of microwaves -- for example, the skin depth is about 2 mm at 10 GHz (Plant 1990) -- Hwang (2012) uses the fraction of whitecap coverage as a proxy of the void fraction in the mixing rule for the evaluation of an effective relative permittivity ε_e. The approach renders the problem of ocean emission of foamy water to 2D (horizontal). The whitecap fraction represents an upper bound of the void fraction because it is equivalent to assuming 100% of air in the depth of microwave influence under the foamy area, whereas the actual air entrainment decreases exponentially with water depth (e.g., Wu 1981; Hwang et al. 1990). The effective relative permittivity ε_e of the air-water mixture is computed with the quadratic mixing rule in a similar way discussed in Anguelova (2008):

$$\varepsilon_e = \left[f_a \varepsilon_a^{1/2} + (1 - f_a) \varepsilon_{sw}^{1/2} \right]^2, \quad (1)$$

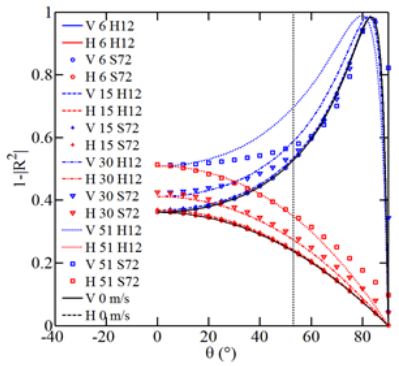

Fig. 1. A comparison of the emissivity of a flat surface covered with foam from wave breaking computed with the equivalent medium approach of Hwang (2012): H12, and Stogryn (1972): S72. The second column in the legend is wind speed in m/s.

where ε_{sw} is the relative permittivity of sea water without whitecaps and ε_a =1 is the relative permittivity of air, and f_a is the air fraction approximated by the whitecap fraction.

Following the analysis presented of Hwang (2012), the formula for f_a is parameterized with the friction velocity u_* using the whitecap data reported in Callaghan et al. (2008):

$$f_a = \begin{cases} \max\left(0, 0.30\left(u_* - 0.11\right)^3\right), & u_* \le 0.40\,\text{m/s} \\ 0.07u_*^{2.5}, & u_* > 0.40\,\text{m/s} \end{cases}. \quad (2)$$

The emissivity calculated with this "equivalent medium" relative permittivity produces similar results as that using the mixing rule applied to the emissivity of foamless sea water area and the emissivity of 100%-foam area as treated in Stogryn (1972) for the H polarization but the two solutions differ significantly for the V polarization in high winds (Fig. 1).

The calculated brightness temperature as a function of wind speed based on the equivalent medium approach is in very good agreement with a global dataset of WindSat microwave radiometer measurements with wind speed coverage up to about 42 m/s (Meissner and Wentz 2009). The WindSat measurements include five microwave frequencies (6, 10, 18, 23 and 37 GHz) for both vertical and horizontal polarizations, and the nominal incidence angle θ is 53° (marked with a dotted line in Fig. 1); see Fig. 3 in Hwang (2012) and Fig. 9 in Hwang et al. (2013).

Presently, there are many GMFs for several microwave frequency bands: Ku, X, C and L. Most of them are for copolarized returns VV and HH. Only the C band offers several versions of the VH GMF. In principle, they can all be used for our task of inferring the surface roughness and wave breaking properties.

3. RESULT AND DISCUSSION

Here we show the results of using the C band co- and cross-polarized GMFs (Hersbach et al., 2007; Mouche et al., 2005; Hwang et al., 2010, 2015). The corresponding NRCS based on the GMFs are shown in Fig. 2a. As mentioned earlier, among these 3 polarizations, HH and VH are more sensitive to wave-breaking in relative terms referenced to the Bragg scattering component. This is especially the case at high incidence angles, where scattering from Bragg resonance surface waves is very low. The wave breaking effects are less visible in VV because of the higher Bragg contribution. Presently, the C-band HH GMF is not yet well consolidated, particularly at high incidence angles because of the limited amount of data from ENVISAT-ASAR analyzed by Mouche et al. (2005). In this work, we use the polarization ratio formulation (*VV/HH*) derived from the RADARSAT-2 (R2) quad-polarization analyses with the directional distribution of the polarization ratio formulated by Mouche et al. (2005), as detailed in Appendix A2 in Hwang et al. (2010). Calculations with GMFs of other frequency bands will be presented elsewhere.

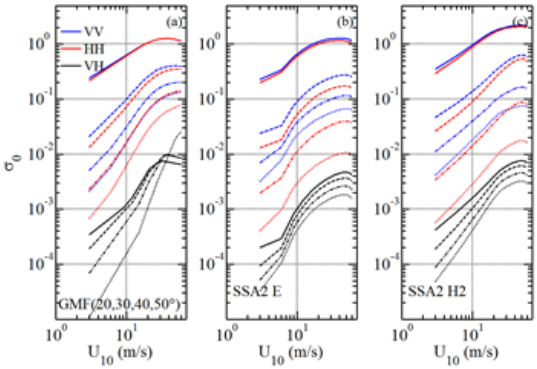

Fig. 2. (a) C-band GMFs for VV, HH and VH used in this study; (b) SSA2 solutions for VV, HH and VH using the E roughness spectrum; and (c) SSA2 solutions for VV, HH and VH using the H2 roughness spectrum.

As a baseline reference, the SSA2 solutions without considering the relative permittivity modification by foam are calculated using the existing E (Fig. 2b) and H (Fig. 2c) roughness spectra: E for Elfouhaily et al. (1997) and H for Hwang et al. (2013). The H spectral model includes swell influence, qualitatively increasing from 1 to 4. The H2 shown in Fig. 2c represents mild swell influence. Both spectral models require the specification of the friction velocity u_* as a function of wind speed U_{10}. There are currently many different formulas of the drag coefficient C_{10} connecting u_* and U_{10}. In the present installation, we use the same formula discussed in Hwang et al. (2013) for both spectral models:

$$C_{10} = 10^{-5}\left(-0.16U_{10}^2 + 9.67U_{10} + 80.58\right). \quad (3)$$

Figure 3 shows the NRCS difference $\delta\sigma_{0pq}$ between GMF and SSA2 solutions (GMF-SSA2), where subscripts p and q are polarizations and can be either V or H. The top row shows the dB difference, and a negative value means that the SSA2 solution is larger than the GMF value. Our basic assumption is that the GMF is the sum of contributions

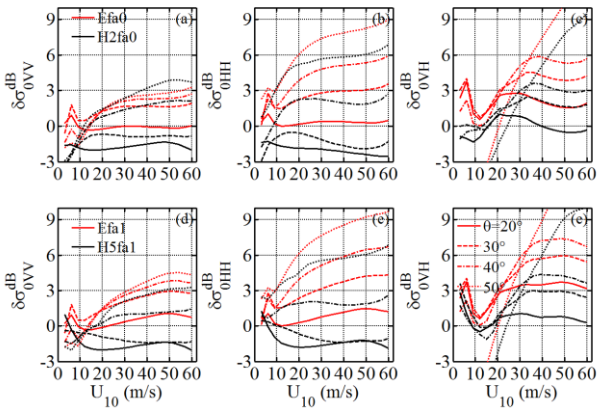

Fig. 3. The difference GMF-SSA2. Top row: the baseline computations without considering relative permittivity modification by foam: (a) *VH*, (b) *HH*, and (c) *VV*; results for E and H2 spectra are displayed. Bottom row shows the corresponding results after including the modifications of relative permittivity and H roughness spectrum.

from roughness and wave breaking, and the SSA2 is the roughness contribution alone. When the GMF is less than SSA2, then either the roughness contribution is over-estimated or the breaking contribution is negative. The former indicates over-specifying the Bragg scale surface roughness. The latter can be from modification of the relative permittivity by the breaking entrained air. A decreased relative permittivity reduces backscattering as a result of decreased reflectivity (Fig.1).

The VV is dominated by Bragg resonance scattering; therefore it is especially useful for evaluating the roughness spectrum models. For the baseline computations (Figs. 3a-c), the SSA2 solutions using the H2 spectral model are larger than the GMF in low and moderate winds (U_{10}≤~12 m/s) for the whole range of incidence angles used in the computation (20° to 50°), and at θ=20° and 30° across the full range of wind speeds. This would indicate an over-specification of the Bragg resonance roughness spectral components. For the C band computations shown here, the Bragg wavenumbers are 76, 111, 143 and 170 rad/m for the four incidence angles 20°, 30°, 40° and 50°, respectively. The SSA2 VV solutions of the baseline computations using the E spectrum is in excellent agreement with GMF at θ=20°. For 30° to 50°, the difference increases toward higher incidence angles.

To further address the discrepancy between modeled results and VV GMF, the relative permittivity modification by the breaking entrained air needs to be implemented. We also need to consider the limited validity of the SSA2 at high incidence angles. The important condition of SSA2 validity is that the tangent of grazing angles of incident radiation shall sufficiently exceed the root mean square (rms) slope of the surface. For high wind speeds, this condition might breakdown at 60° incidence. In any case, the VV comparison can be used for refining the surface roughness spectral model. The H roughness model is constructed with the empirical power law relationship between the dimensionless spectrum $B(k)$ and the dimensionless wind forcing parameter u_*/c:

$$B\left(\frac{u_*}{c};k\right)=A(k)\left(\frac{u_*}{c}\right)^{a(k)} . \qquad (4)$$

The parameters $A(k)$ and $a(k)$ are obtained from a free-drifting wave gauge (FDWG) system (Hwang, 2005). They can also be extracted from microwave radar and radiometer measurements, e.g., see the summary given in Hwang (1997) and Trokhimovski and Irisov (2000), as well as the radar spectrometer analysis of the roughness spectral components using Ku-, C- and L-band GMFs as discussed in Hwang et al. (2013). The previous versions of the H roughness spectral model rely heavily on the in situ FDWG data. The task of roughness model refinement involves the formulation of $A(k)$ and $a(k)$ incorporating the remote sensing data, as shown in Fig. 4.

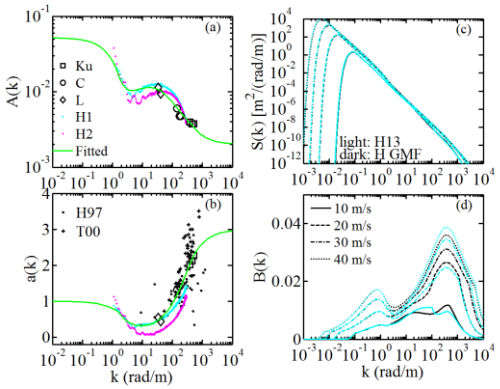

Fig. 4. The parameters (a) $A(k)$, and (b) $a(k)$, for the H spectrum model combining both in situ oceanographic instruments and microwave remote sensing sensors. (c) and (d) are the resulting displacement and dimensionless spectra, respectively. The modified spectra are compared with Hwang et al. (2013).

After implementing the modification of relative permittivity by breaking entrained air and refinement of the surface roughness model incorporating the remote sensing results, the *VV* agreement with GMF improved somewhat for the H spectrum, especially in the low wind portion, but disagreement remains (Figs. 3d-f). As a final step, the ratio of *VV(SSA2)/VV(GMF)* is computed as an *ad hoc* correction of the surface roughness spectrum. The ratio is applied to the *HH* and *VH* SSA2 solutions, and the difference with the GMF represents the breaking contribution (Fig. 5).

The results show a general quadratic to cubic wind speed dependence for U_{10}<~20 to 30 m/s (Fig. 5, upper row). The breaking contribution can be expressed in terms of the equivalent roughness with reference to the Bragg roughness, showing in dB scale in the bottom row of Fig. 5. The relative weighting of the breaking contribution for the

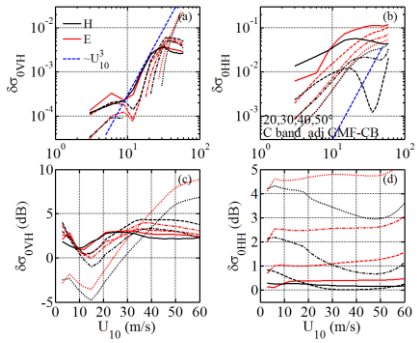

Fig. 5. The final result of wave breaking contribution considering modification of relative permittivity by foam, and adjusting VV to agree with the GMF. Left column: VH, right column: HH; upper row: in log-log scales, bottom row: in dB scales.

HH polarization depends strongly on the incidence angle. In contrast, the incidence angle dependence of the relative breaking contribution is weaker in *VH*. These results are based on our imperfect knowledge of the *HH* and *VH* GMFs. We expect further refinement in the future as the accuracy of GMFs improves. Results of Ku and L band analyses are presented in Hwang and Fois (2015).

4. SUMMARY

Microwave backscattering from the sea surface contains valuable information of the ocean surface roughness and wave breaking that is very difficult to measure using conventional oceanographic instruments. Making use of the property that *VV*, *HH* and *VH* respond to roughness and breaking differently, a method to extract the quantitative roughness and breaking properties is outlined. Basically, the GMFs established from global NRCS measurements are treated as field data of roughness and wave breaking reflected in the interaction of microwave and sea surface. Theoretical solutions of the Bragg resonance scattering from the surface roughness contributions for *VV*, *HH* and *VH* are computed using the SSA2. The *VV* comparison between the GMF and SSA2 solutions is useful for refining the ocean surface roughness spectral model. Once a satisfactory roughness model is obtained, the differences between the GMF and SSA2 solutions can be used to establish an empirical model of surface wave breaking relevant to microwave scattering from the ocean surface.

5. REFERENCES

Anguelova, M. D. (2008), Complex relative permittivity of sea foam at microwave frequencies, *J. Geophys. Res.*, *113*, C08001.

Callaghan, A., G. de Leeuw, L. Cohen, C. D. and O'Dowd (2008), Relationship of oceanic whitecap coverage to wind speed and wind history, *Geophys. Res. Lett.*, *35*, L23609.

Elfouhaily, T., B. Chapron, K. Katsaros, and D. Vandemark (1997), A unified directional spectrum for long and short wind-driven waves, *J. Geophys. Res., 102,* 15781-15796.

Fois, F., P. Hoogeboom, F. Le Chevalier, and A. Stoffelen (2014), Future ocean scatterometry at very strong winds, *IEEE Proc. Int. Geos. Remote Sensing Symp.*, 3886-3889.

Hersbach, H., A. Stoffelen, and S. de Haan (2007), An improved C-band scatterometer ocean geophysical model function: CMOD5, *J. Geophys. Res., 112, C03006*.

Hwang, P. A. (1997), A study of the wavenumber spectra of short water waves in the ocean. Part 2: Spectral model and mean square slope. *J. Atmos. Oceanic Tech., 14*, 1174-1186.

Hwang, P. A. (2005), Wave number spectrum and mean-square slope of intermediate-scale ocean surface waves, *J. Geophys. Res., 110, C10029*.

Hwang, P. A. (2012), Foam and roughness effects on passive microwave remote sensing of the ocean, *IEEE Trans. Geos. Rem. Sens., 50*, 2978-2985.

Hwang, P. A., and F. Fois, 2015: Surface roughness and breaking wave properties retrieved from polarimetric microwave radar backscattering. *J. Geophys. Res*., doi:10.1029/2015JC010782 (in press).

Hwang, P. A., Y.-H. L. Hsu, and J. Wu (1990), Air bubbles produced by breaking wind waves: A laboratory study, *J. Phys. Oceanogr., 20*, 19-28.

Hwang, P. A., B. Zhang, J. V. Toporkov, and W. Perrie (2010), Comparison of composite Bragg theory and quad-polarization radar backscatter from RADARSAT-2: With applications to wave breaking and high wind retrieval, *J. Geophys. Res*., *115*, C08019.

Hwang, P. A., D. M. Burrage, D. W. Wang, and J. C. Wesson (2013), Ocean surface roughness spectrum in high wind condition for microwave backscatter and emission computations, *J. Atmos. Oceanic Tech., 30*, 2168-2188.

Hwang, P. A., A. Stoffelen, G.-J. van Zadelhoff, W. Perrie, B. Zhang, H. Li, and H. Shen (2015), Cross polarization geophysical model function for C-band radar backscattering from the ocean surface and wind speed retrieval. *J. Geophys. Res*, 120, 893-909, doi:10.1029/2014JC010439, 2015.

Mouche, A. A., D. Hauser, J. Daloze, and C. Guerin (2005), Dual-polarization measurements at C-band over the ocean: Results from airborne radar observations and comparison with ENVISAT ASAR data, *IEEE Trans. Geos. Rem. Sens., 43*, 753-769.

Plant, W. J. (1990), Bragg scattering of electromagnetic waves from the air-sea interface, in *Surface waves and fluxes, Vol. II – Remote sensing*, eds. G. L. Geernaert and W. L. Plant, 41-108.

Stogryn, A. (1972), The emissivity of sea foam at microwave frequencies, *J. Geophys. Res., 77*, 1658–1666.

Trokhimovski, Y. G., and V. G. Irisov (2000), The analysis of wind exponents retrieved from microwave radar and radiometric measurements. *IEEE Trans. Geosci. Remote Sens., 38*, 470–479.

Voronovich, A. G. (1994), Small-slope approximation for electromagnetic wave scattering at a rough interface of two dielectric half-spaces, *Waves Random Media, 4*, 337-367.

Wu, J. (1981), Bubble populations and spectra in near-surface ocean: Summary and review of field measurements, *J. Geophys. Res., 86*, 457-463.